Journal of Applied Polymer Science

Pressure-Activated Microsyringe Composite Scaffold of Poly(L-lactic acid) and Carbon Nanotubes for Bone Tissue Engineering

Giovanni Vozzi,[1,2] Claudio Corallo,[2] Chiara Daraio[3]

[1]Department of Chemical Engineering, Industrial Chemistry and Materials Science, University of Pisa, Via Diotisalvi 2, Pisa 56126, Italy

[2]Interdepartmental Research "E. Piaggio", University of Pisa, Via Diotisalvi 2, Pisa 56126, Italy

[3]Engineering and Applied Science, California Institute of Technology, Pasadena, California 91125

Correspondence to: G. Vozzi (E-mail: g.vozzi@centropiaggio.unipi.it)

ABSTRACT: Tissue engineering is an innovative interdisciplinary field in which bioengineers and life scientists try to regenerate and reproduce natural tissues through the use of biodegradable structures, called *scaffolds*, with the aim of mimicking the specific tissue extracellular matrix (ECM). Carbon nanotubes (CNTs) offer a natural platform for obtaining composite microfabricated scaffolds thanks to their excellent mechanical properties and their good biocompatibility. In this study, we microfabricated three-dimensional (3D) scaffolds by mixing poly(L-lactic acid) (PLLA) and multiwalled carbon nanotubes (MWCNTs) for bone tissue engineering. We measured their mechanical properties and studied their biocompatibility with human fetal osteoblasts (hFOB 1.19). The 3D microfabricated PLLA/MWCNTs nanocomposite scaffolds showed higher stiffness and cell viability than the pure 3D microfabricated PLLA scaffolds. The results of this preliminary work suggest that biopolymer/CNT microcomposites and nanocomposites could be used as effective building blocks to replace ECMs in bone tissue engineering applications. The final goal is the creation of innovative scaffolds for implants and tissue regeneration. © 2012 Wiley Periodicals, Inc. J. Appl. Polym. Sci. 129: 528–536, 2013

KEYWORDS: bioengineering; biomaterials; mechanical properties

Received 7 May 2012; accepted 21 June 2012; published online 26 July 2012
DOI: 10.1002/app.38235

INTRODUCTION

A central theme in the design of tissue engineering scaffolds is to understand the relationship between the scaffold properties and biological functions.[1] During tissue development, cells constantly decode and release different morphogenetic factors to their surroundings. In response to these, cells activate their cell processes [proliferation, differentiation, migration, degradation/production of the extracellular matrix (ECM), etc.]. On the basis of our knowledge of cell–ECM interactions in native tissues,[2] it should be possible to design scaffolds that are able to promote tissue formation through systematic changes in one or more chemical and/or physical properties. Living cells and tissues, however, are not simple linear systems. The complex role that ECM structures play in the generation of cellular and tissue processes can be thought of as a multiband signal to which different cell types may exhibit radically different sensitivities.[3] In bone structure, the ECM allows the optimal distribution of mechanical stresses to stimulate bone cells to activate their cell processes and to induce local points where the stress is greater than that at failure.

There are several approaches to bone tissue engineering, but all involve one or more of the following key ingredients: harvested cells, recombinant signaling molecules, and three-dimensional (3D) matrices.[4] The most commonly used approach involves seeding cells and signaling molecules (e.g., protein growth factors) in highly porous biodegradable matrices (or scaffolds) preformed into the shape of the desired bone.[5] Once the seeded cells are cultured and colonize the matrices, they are implanted directly on the defect to induce and direct the growth of new bone.

Normally, cells are cultured in an artificial environment, where they can adhere and replicate to form larger colonies of cells for applications such as diagnostic testing.[6] These colonies, however, do not become organized into tissues or organs that could then be implanted back into the patient.[7] Cell colonies need external cues or signals to grow into functional 3D tissues or organs.[8] In the body, cells are constantly subjected to mechanical, electrical, structural, and chemical cues that signal the cells about what they should be doing. If these signals are not properly received or processed because of disease or trauma, the cells

© 2012 Wiley Periodicals, Inc.

dedifferentiate (i.e., become nonspecific cell types), become disorganized, and eventually die.[9]

A valid approach is to combine different materials to produce a composite structure. Composite scaffolds are expected to be physically and biologically superior to single-material based scaffolds, so the properties of a composite scaffold may be tuned by the mixture of different materials in various percentages.[10] The composition, the relative ratio of constituent materials, and the scaffold porosity can affect bone formation. Usually, an increase in the solid material present in the scaffold (lower porosity), caused by a decrease in the pore height and pore width, is one of the bases of improved mechanical behavior in composite scaffolds.[11] Hydroxyapatite (HA) has been used as a primary material in combination with another material, such as tricalcium phosphate (TCP), poly(lactic-*co*-glycolic acid) (PLGA), or chitin, to produce various composite scaffolds.[12] It was reported that scaffolds with different ratios of HA to TCP loaded with MSCs showed different extents of bone formation *in vivo*.[13] Composites in which the HA/TCP ratio was designed to coordinate scaffold degradation with tissue deposition seemed optimal for the promotion of the greatest ectopic bone formation.[13]

In recent years, bone scaffolds have been realized with composite materials based on carbon nanotubes (CNTs).[14,15] CNTs offer a natural platform for obtaining composite microfabricated scaffolds because of their excellent mechanical and electrical properties, coupled with a good biocompatibility.[16] The extraordinary mechanical properties of CNTs make them very attractive and promising as reinforcing fillers for the production of a new generation of tissue substitutes. Experimental data reveal that CNTs dispersed in a polymer matrix significantly improve its mechanical properties.[17–20]

Although mechanical reinforcement was the initial motivation for their use, there is evidence that CNTs can accelerate and direct cell growth. The topic of the biocompatibility of CNTs is still an openly debated issue that needs further investigation. The chemical inertness of CNTs allows them to have a quite low toxicity, except for inhalation-related toxicity. However, it is fundamental to purify nanotubes from metal catalysts and graphite particles because they have been shown to be responsible, at least in part, for the toxicity in the preparation of CNTs.[21] Several *in vitro* studies have examined the interactions between CNTs or nanocomposites and animal or human cells. It has been shown that a collagen matrix with embedded single-walled carbon nanotubes (SWCNTs) sustained a high cell viability of smooth muscle cells.[22] Zanello et al.[23] examined the proliferation and function of osteoblast cells seeded onto five differently functionalized CNTs.

CNTs have also been used to create electrically conductive polymers and tissue scaffolds with the capacity to provide controlled electrical stimulation. It has been reported that current-conducting CNT/polymer composites promoted various osteoblast cell functions. With the application of alternating current to these nanocomposites, increases in the osteoblast proliferation of 46% and in the calcium deposition of 307% have been observed.[24] This result suggests that CNT-based composites may be used to stimulate bone formation. In a previous study, we used impedance techniques to measure the effects of media and cell cultures on CNT composite films. We showed that cell adhesion could be distinguished by the interpretation the results of the impedance characteristics.[25] In the presence of cells, impedance changes were around eight times that without cells. Thus, the use of CNTs could be correlated with adhesion, spreading, and changes in the cell density. Considering recent publications, we feel that the use of CNTs for tissue engineering appears to be a challenging but, on the other hand, potentially rewarding perspective for the development of a novel generation of engineered biomaterials.

In this article, we describe the design, fabrication, and testing of 3D cell scaffolds based on poly(L-lactic acid) (PLLA)/multiwalled carbon nanotubes (MWCNTs) composites for bone tissue engineering. We selected specific microstructural topologies to improve the overall mechanical properties of the scaffolds and to mimic the topological features of bone tissue with MicroCT scans of sponge bone. The composite materials were processed with a pressure-activated microsyringe (PAM) microfabrication technique that allowed the direct formation of the desired microstructures. Uniform films (used as control samples) and PAM scaffolds were mechanically tested to measure their stiffness as functions of the MWCNT concentration and the different topologies. The PLLA/CNT ratio in the composite scaffolds was tuned to reproduce the mechanical behavior of bone tissue on the basis of the results obtained from mechanical testing. Cell testing was performed with human fetal osteoblasts (hFOB 1.19) cells to analyze whether the composite material and scaffold were able to induce cell differentiation into mature osteoblast phenotypes.

EXPERIMENTAL

Polymer

The biodegradable polymer used in this study was PLLA (NP Pharm, Bazainville, France), prepared at concentration of 0.2 g/mL in a chloroform solution. We examined the surface and bulk properties of PLLA spin-coated films and microfabricated scaffolds in an earlier study.[26] We showed that the surface charge density, dielectric constant, morphology, contact angle, porosity, and elastic modulus of the polymer were suitable for cell adhesion.[26]

CNTs

In this study, we used MWCNTs to fabricate the PLLA/CNT composite scaffolds because of their suitable mechanical properties. In particular, MWCNTs present a higher elastic modulus than SWCNTs;[27] this allows the realization of rigid composite scaffolds with mechanical properties similar to those of bone structure. Vertically aligned forests of CNTs were synthesized with a thermal chemical vapor deposition system consisting of a two-stage tube furnace. The furnace accommodated a quartz tube 30 mm in diameter and 1000 mm long with a 200-mm preheating zone and a 500-mm heating zone. The temperature of the preheating zone was 80°C, and the heating zone was maintained at 825°C. The CNTs were grown on SiO_2 substrates with a floating catalyst technique. A mixture of Fe catalyst (ferrocene) and a carbon source (toluene, 0.02 g/mL) was injected in the preheating zone at a rate of 5 mL/15 min. Argon was used as a carrier gas for the solution at a flow of 800 sccm. The grown CNTs were about 800 nm long and had an outer diameter ranging from 15 to 50 nm. After growth, the CNTs were

Table I. Acronyms of the Nanocomposite Suspensions and Their Final Concentrations

Abbreviation	PLLA final concentration (mg/mL)	CNT final concentration (mg/mL)	CNT relative weight (%)
PLLA	100	0	0
PLLA-A[a]	100	6.25	11
PLLA-B	100	12.5	20
PLLA-C	100	37.5	42

[a]This solution was used for the microfabricated scaffolds.

removed from the substrates with a razor blade and were dispersed in solution.

Film and Scaffold Fabrication

To obtain a uniform dispersion of CNTs in the polymer matrix, we used a dual-solvent approach similar to the one described in our previous work.[28] With this method, multiwalled CNTs were dispersed in benzene with a pulsed sonicator (Vibracell, Sonics, Milan, Italy) for 1 min at 1 Hz in 3D concentrations: 12.5 mg/mL (solution A), 25 mg/mL (solution B), and 75 mg/mL (solution C). Then, the three solutions were mixed with PLLA in a 1:1 ratio and sonicated. This resulted in three suspensions with the concentrations and acronyms provided in Table I. The three CNT–PLLA suspensions were tested together with pure PLLA polymer for comparison. Suspensions B and C were selected on the basis of the mechanical properties of their spin-coated films. The selection was based on the stiffness of the final suspension (chosen to closely approximate the mechanical behavior of bone) and its viscosity (chosen within a range that allowed PAM fabrication). The PLLA–CNT suspension flat films were realized by a spin-coating technique (Suss Microtech, Neuchatel, Switzerland). The PLLA-A solution (0.1 g/mL PLLA and 12.5 mg/mL CNT) was used because of its known characteristics, which allowed the realization of high-fidelity structures.[29]

The PAM deposition method was described previously.[30] It consisted of a stainless steel microsyringe with a capillary tip of 5–20 mm, through which the suspension was extruded by the application of pressure from a compressed and filtered air supply. To improve the extrusion properties, 2 mL of Tween was added to each milliliter of suspension; this helped us maintain a uniform dispersion during the deposition process.

The vertical position of the syringe was controlled by the *z* motor of a three-axis positioner, whereas the substrate was mounted on the *x* and *y* axes and moved relative to the syringe. Purposely written software allowed almost any type of structure to be deposited in sequential layers simply by the translation of a black and white jpeg or bitmap image into a sequential list of linear coordinates; this could be used to direct the position of the *x* and *y* motors. For example, in earlier studies, we microfabricated layers consisting of spiral, square, hexagonal, and octagonal grids and fractal branches.[31] The line width of the deposited structure could be modulated by variation of the polymer viscosity, deposition speed (the velocity of the x and y motors), tip diameter, or applied pressure.[30]

For this study, we realized four types of scaffolds composed of layers with different geometrical structures. The first scaffold consisted of a square grid layer, the second scaffold consisted of a hexagonal grid layer, the third scaffold consisted of a tessellation of octagonal and rhomboidal elements, and the last scaffold consisted of a three-layer assembly that combined all of the previous geometries in the sequential layers. This bonelike scaffold was shown to closely mimic the microstructure of bone.[32] All four scaffolds are shown in Figure 1. The scaffolds were deposited on 3 × 3-cm^2 clean glass slides. The two-dimensional grids

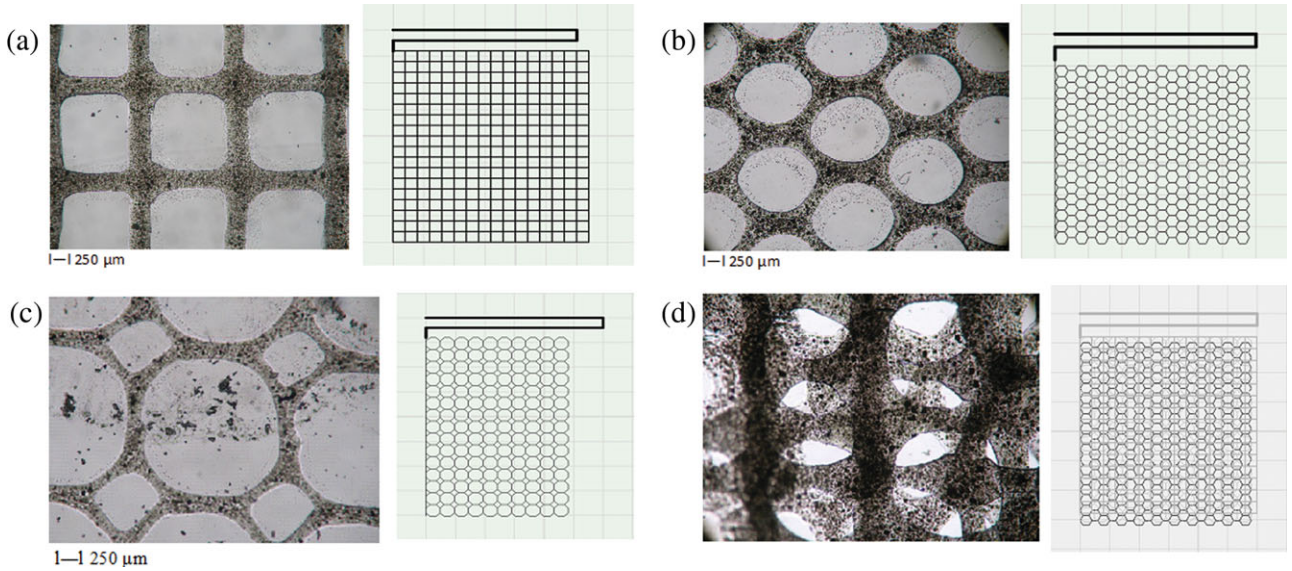

Figure 1. Light microscopy of the PAM PLLA/MWCTs nanocomposite scaffolds with different topologies and their respective computer-aided design drawings: (a) hexagonal, (b) square, and (c) octagonal cell grids and (d) 3D bonelike scaffold obtained by the composition of the aforementioned three different layers. [Color figure can be viewed in the online issue, which is available at wileyonlinelibrary.com.]

($1\ cm^2$) were composed of square, regular hexagonal, and octagonal elements with side lengths of 500 μm and line thicknesses of 50 μm.

To fabricate the 3D scaffolds, we deposited a water-soluble polymeric spacer (2 mg/mL, Hydrofilm, Lucca, Italy) of about 10–20 μm on top of the first layer of the PLLA–CNT suspension. After drying, we deposited a second identical layer of PLLA–CNT suspension, slightly shifted with respect to the first layer, and then a second polymeric spacer. This procedure was repeated for all three layers to produce the final structure. At the end of the microfabrication process, the scaffolds were dipped in water to dissolve the polymer spacer and lift them off of the substrates. After this process, the scaffolds were dried and could be used for the experiments.

Mechanical Tests

Stress–Strain. The mechanical properties of the scaffolds and films were measured with an isotonic transducer (model 7006, UGO Basile Biological Research Apparatus, Comerio (VA), Italy), where the applied force had a resolution of 1 mN. The scaffolds and films with dimensions of 2 cm in length and 0.5 cm in width were specifically fabricated for the measurements. Images of each scaffold were recorded through an optical microscope equipped with a digital camera to obtain data on the initial dimensions and geometry. Two small strips of transparent acetate ($5 \times 2.5\ mm^2$) were glued to either side of one end of the scaffold, and a small hole was pierced in the transparency to attach the sample to the transducer lever. The other end was held firmly by a small clamp. The applied force acted along the direction of the maximal length of the structures, and the structures were subjected to tension.

During the stress–strain tests, the applied weights were changed every 3 min, and then, the elastic modulus of each structure was calculated from the slope of the initial linear portion of the resulting curve.

Creep tests were performed with the same instrument and the application of a load corresponding to a strain of 5% of the maximum elastic strain of the structure under dry conditions. The load was applied for 1 h, and the relaxation was analyzed for a further 1 h after its removal. Ten samples were used per test.

Nanoindentation Test. Nanoindentation tests were performed on both the PLLA and PLLA/MWCNT scaffold surfaces with a flat punch with a diameter of 97 μm in an MTS Nano G200 (Agilent). Nanoindentation tests provided information on the mechanical responses on the surfaces of the scaffolds. The evaluation of the surface stiffness of the different scaffolds was important in relation to cell adhesion and proliferation. The nanoindentation tests included in this study were performed at three different strain rates: 0.01, 0.1, and $1\ s^{-1}$.

Cell Culture. hFOB 1.19 (ATCC) presents a temperature-switching gene that regulates proliferation and differentiation. In particular, cells exhibit rapid proliferation when they are cultured at 33.5°C, whereas no proliferation occurs at 37°C. At this temperature, these cells express alkaline phosphatase activity and a mature osteoblastic phenotype.[33]

Cells were grown in a controlled atmosphere (5% CO_2, temperature = 34°C) in a 1:1 mixture of Ham's F12 and Dulbecco's modified eagle medium (DMEM) (Invitrogen) with 2.5 m*M* L-glutamine (without phenol red) supplemented with 10% fetal bovine serum (Hyclone, 925 West 1800 South Logan, Utah 84321), 0.3 mg/mL G418, and 1% antibiotics (penicillin–streptomycin, Gibco, Life Technologies Corporation, Milan, Italy). After thawing, the cells were routinely split (1:4) every 2–3 days. The cells incubated at 39.5°C showed rapid differentiation into mature osteoblasts.

Before cell seeding, the scaffolds and films were sterilized in 70% ethanol for 2 h, washed in phosphate-buffered saline (PBS) and 70% ethanol for 2 h, placed under UV irradiation for 10 min for each side, and incubated for 10 min with a 0.3% murine collagen solution, in acetic acid (Sigma-Aldrich Italia, Milan, Italy) for 2 h, and then in a complete cell culture medium for 1 h. The medium was then discarded, and the hFOB 1.19 cells were detached with 0.25% trypsin in 1m*M* ethylene diamine tetraacetic acid and plated (in triplicate) onto the samples and in 24-well polystyrene tissue culture plates as controls at a density of 3×10^4 cells/cm^2. To assess the CNT cytotoxicity, spun films for each solution were used in the cell culture experiments. As far as the PAM scaffolds were concerned, the biocompatibility was assessed only on the microfabricated three-layer structures that mimicked the bone microstructure.

Viability Assay and Measurement of Cell Density

After incubation (for 24, 48, and 72 h), the culture medium was removed from each well; 200 μL of CellTiter-Blue reagent (0.1 mg/mL in DMEM without phenol red) was added to each sample. The multiwelled plates were incubated at 39.5°C for at least 4 h. Viable cells continuously converted resazurin to resorufin, thereby generating a quantitative measure of viability and cytotoxicity. After that time, the multiwelled plate was read spectrophotometrically (Tecan Infinite M1000, Tecan, Mannedorf, Switzerland) at 560 and 690 nm, and the cell viability was quantified. The measured values are expressed as a percentage over that of the control cultures (tissue culture plates), and the data reported here represent the means and standards deviations obtained from at least three different experiments.

To measure the density of cells adhered on the composite structures, after culturing times of 24, 48, and 72 h, the cells adhered on the scaffold were detached with a 1% trypsin solution in PBS, and the cell suspension was analyzed with a Burker chamber, Magapor, Zaragozza, Spain. For each sample, three measurements of cell suspension were performed.

Scanning Electron Microscopy (SEM)

For the SEM analysis, all of the culture specimens were fixed in 2% glutaraldehyde in 0.1*M* cacodylate buffer (pH 7.4), postfixed in 1% osmium tetroxide, dehydrated in increasing ethanol concentrations, critical point dried (CPD) dried, mounted on aluminum stubs, and gold-sputtered. All specimens were observed with a Philips XL20 microscope (SEMTech Solutions, Inc 6 Executive Park Drive, North Billerica, Ma 01862).

Statistical Analysis

Statistical analysis was performed with an analysis of covariance for a comparison of trends (Matlab Statistics Toolbox, The

Applied Polymer SCIENCE

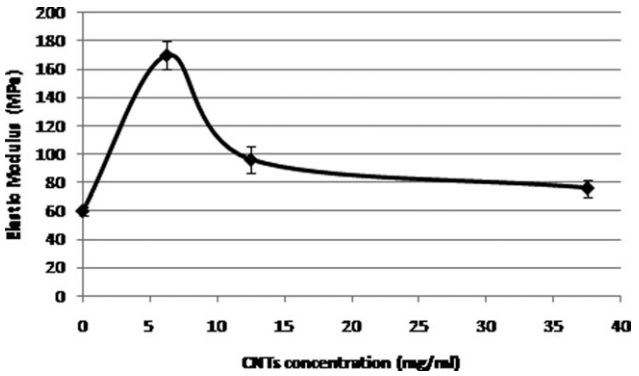

Figure 2. Elastic modulus values of the composite spin-coated films as a function of the MWCNT concentration. The errors were on the order of 5%.

MathWorks, Inc. Natick, Massachusetts). A p value of less than 0.05 was considered to be statistically significant. Each data point is represented as the mean and standard deviation of 10 samples.

RESULTS

Mechanical Tests

The Young's moduli of the composite films as function of the CNT concentration are reported in Figure 2. The results show that the elastic modulus initially increased with increasing CNT concentration until the concentration reached a critical value of 6.25 mg/mL. After this concentration, the elastic modulus decreased rapidly, reaching values close to that of pure PLLA. This behavior could have been due to the electrostatic nature of CNT. When the CNT concentration was too high, the polymer/CNT solution presented an inhomogeneous dispersion, which led to an abrupt decrease in the elastic modulus and in increase in the fragility.[20,34,35]

Figure 3 shows how the stress–strain behavior of the scaffolds was influenced by its topology. If we assumed that the scaffold behaved similarly to a textile, when a load was applied to it, there was first a rearrangement of its weft. The structure responded by realigning the fibers in the direction of the applied load. For this reason, there were differences between the different geometries; in fact, because the octagonal grid had a higher density of lines than the square or hexagonal grid, it presented greater resistance to deformation. The square grid was the least stiff because it had the lowest density of lines. Moreover, the patterns with small line widths had lower yield stresses than the ones with bigger line widths. Therefore, by changing the geometry, we could modulate the mechanical properties of the microstructures. The elastic modulus of the pseudo-bone polymeric structure was an average of the three elastic moduli of the single monolayers that composed it.

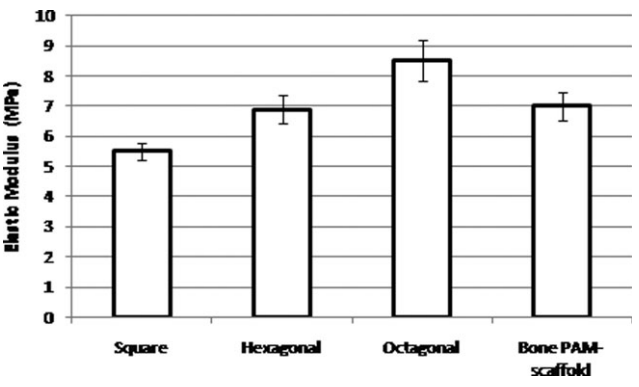

Figure 3. Elastic modulus as a function of the type of PLLA/MWCNT composite for various PAM scaffold topologies. The t test showed that the experimental data were statistically different ($p < 0.05$).

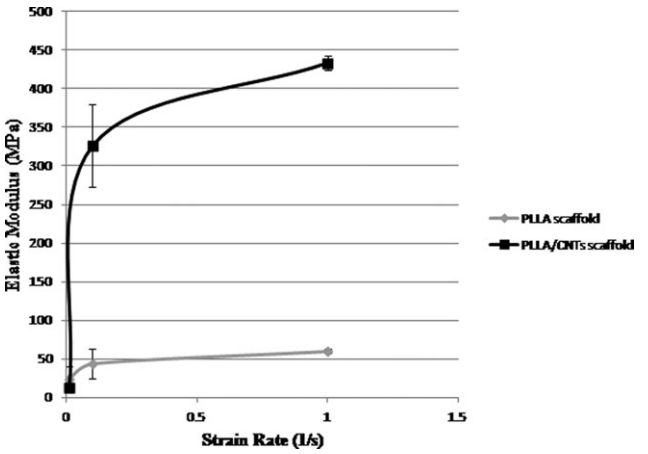

Figure 4. Compression behavior of the PLLA and PLLA/MWCNT bone-like scaffold.

Nanoindentation Test. The results revealed the same behavior for the PLLA and PLLA/CNT scaffolds, and this may have been due to the fact that the low percentage of MWCNTs in the composite scaffolds did not affect the viscoelasticity of the biopolymer. On the other hand, the Young's modulus of the composite PLLA/MWCNT scaffolds in comparison with that of pure PLLA scaffolds was seven times higher, as shown in Figure 4.

Cell Test. All of the composite films showed good cell compatibility, with a value from the viability test of higher than 75% with respect to the control [Figure 5(a)]. By analyzing the vitality data obtained from the cells seeded onto the spun films, we observed that the presence of CNTs affected the cell viability, either on the film or on the scaffold. Moreover, the cells seeded onto the scaffold with or without CNTs showed a larger viability than those seeded onto the spun films. At different times, the cell density statistically increased [Figure 5(b)], so this result suggests that the cells on the PLLA/CNT scaffold were more viable. Thus, the mechanical properties and the topology were two important cues for the cell activity.

The SEM analyses revealed that the topology and CNT presence had a noticeable influence on the film morphology. The SEM morphological analysis of the osteoblasts grown on the spun films showed that the cell shape and spreading were dependent on the surface topography. On the PLLA/CNT spun films, the cells tended to assume an elongated aspect and to extend along protrusions to anchor themselves at distance on the smooth surface [Figure 6(a)]. Osteoblasts cultured on the PLLA spun films showed a more spheroid morphology and did not present long protrusions [Figure 6(b)]. The features of the cells seeded onto the PAM scaffolds with or without CNTs were comparable

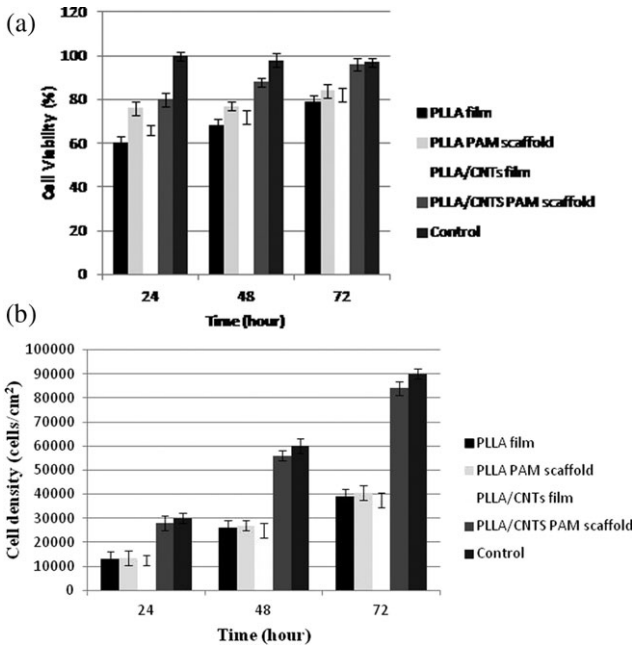

Figure 5. (a) Cell vitality and (b) cell density values of various spin-coated PLLA and PLLA/CNT composites and 3D bonelike scaffolds. The *t* test showed that the experimental data were statistically different ($p < 0.05$).

to those seeded onto the PLLA/CNT films, whereas in the pores, the cells were elongated and exhibited long protrusions [Figure 6(c,d)].

DISCUSSION

3D porous scaffolds promote new tissue formation by providing a surface and a void volume that promotes the attachment, migration, proliferation, and desired differentiation of connective tissue progenitors throughout the region where the new tissue is needed.[36,37] The most important variables in scaffold design and fabrication are the material of which it is made, the 3D architecture, the surface chemistry, the mechanical properties, and the cell culture or physiological environment that regulates its degradation.[38–41] Moreover, the influence of the polymer scaffold architecture on the degradation process has been largely debated in literature. For example, PLGA films degrade faster than porous PLGA scaffolds because a lower porosity accelerates the PLGA degradation process.[42] Researchers also reported that the degradation of porous poly(L-lactic acid) (PLLA) scaffolds *in vitro* is faster for thicker walls than thinner ones because of the autocatalysis of lactic acid.[43] When one starts from these assumptions, it is important to choose the right polymer and its related mechanical and structural properties according to the target tissue. In the case of bone tissue engineering, scaffolds should degrade in concert with the formation of newly generated bone to provide a smooth transition from scaffold to tissue.[44] Furthermore, numerous authors have shown the properties of PLLA scaffolds that suggest that they are suitable for tissue engineering applications.[45,46] PLLA represents a very good choice for bone tissue engineering, where a high mechanical strength and toughness are required.[47] This polymer can be formed into films, fibers, tubes, and matrices with standard processing techniques, such as molding, extrusion, spinning, and solvent casting. Its total degradation time is about 24 months. Although in our previous studies[20] we observed the properties of polycaprolactone (PCL) polymer in bone tissue engineering, we found that PCL showed a remarkably slow degradation rate (from 6 months up to 3 years).[48] Thus, the need to choose a polymer with the right degradation time coupled with the best mechanical properties. In this study, we realized scaffolds with different topologies made up of PLLA and CNTs and obtained, at the same time, a structure that reproduced the typical geometrical features of the bone structure and mechanical properties more similar to those of native bone. In this way, the structure could attract stem cells and induce their differentiation toward the osteogenic phenotype.[49] We showed that with a change in the ratio between the CNTs and PLLA, the intrinsic mechanical properties of the nanocomposites films could be varied between 60 and 170 MPa under tensile stresses, whereas in our previous study with PCL and CNTs,[20] the mechanical properties could be varied between 10 and 75 MPa. Therefore, we believe that because of their improved mechanical properties, the PLLA/CNT nanocomposites are more suitable than PCL/CNT nanocomposites for bone tissue engineering applications. We also found a limit in the CNT concentration that could be added to the polymer matrix; beyond this concentration, the elastic modulus decreased rapidly, reaching values close to that of pure PLLA. These results were in agreement with former results on carbon black particles in the PLLA matrix.[50,51] Kim et al.[50] showed that the application of low shear forces could induce the agglomeration of initially well-dispersed carbon black particles, explaining that the shear forces provided to the particles sufficient kinetic energy to overcome the repulsive interactions of the electric double layers. At the same time, agglomerates could be disrupted by high shear forces. The massive aggregation of CNTs apparently reduced the mechanical performance of the composites because of the disruption of interfacial interaction between the CNTs and the polymer matrix. We also observed that increasing the loading amount of nanotubes in these composites caused a significant increase in the stiffness, which eventually led to brittle fracture, as indicated by a lower elongation at break. It is important to note that the protocol adopted for mixing the PLLA and CNTs allowed us to obtain a uniform dispersion, similar to those reported by Whulanza et al.[25]

For this study, we selected the nanocomposite with the highest elastic modulus to microfabricate PAM scaffolds with different geometries but always with the same porosity, around 65–70%. Figure 3 illustrates how the intrinsic stiffness of the material could be coupled to a given topology to enable modulation of the gross mechanical behavior of the composite scaffold.

It is well known that the mechanical properties of fibrous materials and composites depend on the architecture of fibers.[38] If we assume that the scaffolds behaved similarly to a textile, when a load was applied to them, first there was a rearrangement of its weft. The structure first responded by aligning the filaments in the direction of the applied load. For this reason, there was a difference between the different geometries; in fact, because the octagonal grid had a high density of filaments oriented in

Applied Polymer SCIENCE

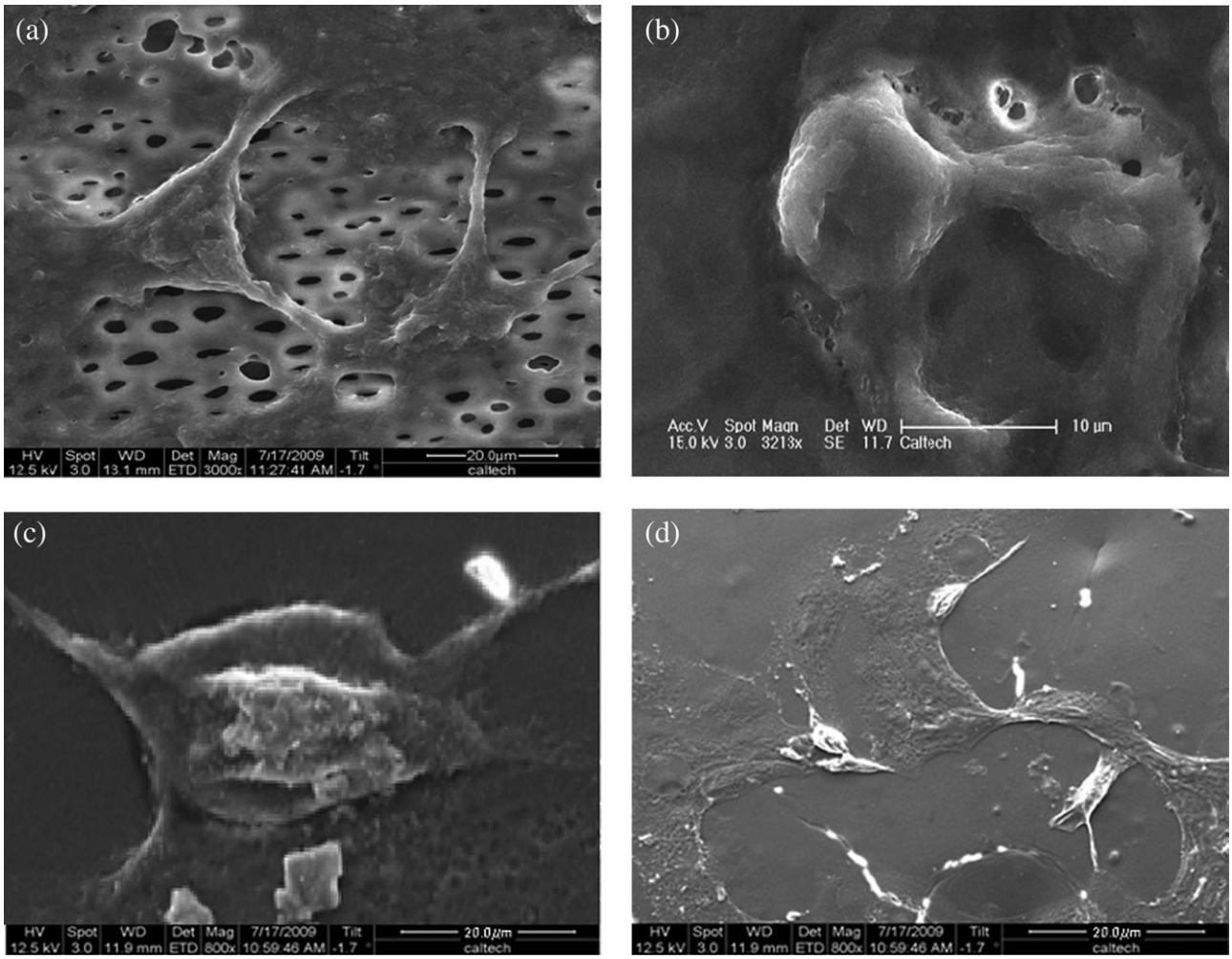

Figure 6. SEM micrographs of hFOB 1.19 cells cultured on the (a) PLLA/CNT spun film, (b) PLLA spun film, (c) PLLA/CNT 3D bonelike PAM scaffold, and (d) PLLA 3D bonelike PAM scaffold.

several directions, it resisted deformation (ca. 8 MPa). On the other hand, the square grid showed a decreased resistance (ca. 4 MPa) because it had a low filament density, with only two orientations. The stiffness of the 3D bonelike scaffold fell between the two extremes. Overall, the mechanical properties of the scaffolds were influenced first by the material employed and second by the geometry of the scaffold. A more complex geometry endowed more viscous properties to the scaffold and may be more suitable for tissue engineering because these cells would not be subject to mechanical shock upon loading and unloading.

Furthermore, during the nanoindentation test, we observed that the presence of CNTs increased the elastic modulus of the structure. Moreover, the nanoindentation tests performed at different strain rates allowed us to analyze which elastic modulus the cell perceived locally of the structure and also whether the composite scaffold could be easily indented by the cells. As it is possible to see from Figure 4, only for shear rates higher than the physiological ones did the composite structure become more rigid than normally happens in the body.

There have been several reports describing the influence of CNTs on the behavior of different cells; however, the exact mechanisms by which they act are still unclear. Our study showed that altogether, the PLLA/CNT nanocomposites could sustain osteoblast proliferation. Our data suggest that osteoblast viability depended on the intrinsic rigidity of the substrate, as reported by Discher et al.,[53] but was also modulated by the architecture and morphology of the substrate. The cell behavior on the 3D bonelike scaffold was comparable to that on the control. Because the scaffold microstructure (porosity, mean pore size, pore shape, interconnectivity, and specific surface area)[54,55] and mechanical properties significantly influenced the cell behavior (e.g., adhesion and growth), our observations confirmed that the proposed 3D bonelike scaffold may represent an interesting physical support structure for bone tissue engineering applications.[56]

CONCLUSIONS

In this study, we realized and characterized PLLA/CNT composite microfabricated scaffolds for bone tissue engineering

applications using a PAM system The results obtained show that the CNTs/polymer composites structures exhibited an improvement in the mechanical properties that could be tailored through changes in the topology of the structure. The CNTs were effective reinforcements in terms of mechanical strengthening in biodegradable scaffold applications. From cell testing, we observed that the cell behavior on the 3D bonelike scaffold was comparable with that on the control. On the basis of these results, the CNT composite PAM scaffolds could represent a valid support for bone regeneration. Moreover, in future studies, thanks to the high porosity of the PLLA/CNT scaffolds, it could be reasonable to functionalize CNTs for drug-delivery applications. In this context, the modification of the physical properties and drug-delivery characteristics through the blending of three major polymers (PLLA, PLGA, and PCL) could further improve the field of nanocomposite materials for bone tissue engineering applications.

ACKNOWLEDGMENTS

This work is supported by the Institute for Collaborative Biotechnologies, under contract W911NF-09-D-0001 with the Army Research Office. We thank Dr. Abha Misra and Dr. Jordan R. Raney, Division of Engineering and Applied Science, and Prof. Chin-Lin Guo, Division of Bioengineering and Applied Physics, California Institute of Technology, Pasadena, CA.

REFERENCES

1. Carletti, E.; Motta, A.; Migliaresi, C. *Methods Mol. Biol.* **2011,** *695*, 17.
2. Latif, N.; Sarathchandra, P.; Taylor, P. M.; Antoniw, J.; Yacoub, M. H. *Cell. Biochem. Biophys.* **2005,** *43*, 275.
3. Daley, W. P.; Peters, S. B.; Larsen, M. J. *Cell. Sci.* **2008,** *121*, 255.
4. Bueno, E. M.; Glowacki, J. *Nat. Rev. Rheumatol.* **2009,** *5*, 685.
5. Lee, S. H.; Shin, H. *Adv. Drug Delivery Rev.* **2007,** *59*, 339. Published Online: Apr 12, 2007.
6. Fleming, J. E., Jr.; Cornell, C. N.; Muschler, G. F. *Orthop. Clin. North Am.* **2000,** *31*, 357.
7. Kimelman, N.; Pelled, G.; Gazit, Z.; Gazit, D. *Regen. Med.* **2006,** *1*, 549.
8. Schumann, D.; Ekaputra, A. K.; Lam, C. X.; Hutmacher, D. W. *Methods Mol. Med.* **2007,** *140*, 101.
9. Mayr-Wohlfart, U.; Fiedler, J.; Günther, K. P.; Puhl, W.; Kessler, S. J. *Biomed. Mater. Res.* **2001,** *57*, 132.
10. Gloria, A.; De Santis, R. J. *Appl. Biomater. Biomech.* **2010,** *8*, 57.
11. Domingos, M.; Chiellini, F.; Gloria, A.; Ambrosio, L.; Bartolo, P.; Chiellini, E. *Rapid Prototyping J.* **2012,** *18*, 56.
12. Boccaccini, A. R.; Blaker, J. J. *Expert Rev. Med. Devices.* **2005,** *2*, 303.
13. Siggers, K.; Frei, H.; Fernlund, G.; Rossi, F. J. *Biomed. Mater. Res. A.* **2010,** *94*, 877.
14. Sahithi, K.; Swetha, M.; Ramasamy, K.; Srinivasan, N.; Selvamurugan, N. *Int. J. Biol. Macromol.* **2010,** *46*, 281.
15. Shi, X.; Sitharaman, B.; Pham, Q. P.; Liang, F.; Wu, K.; Billups, E. W.; Wilson, L. J.; Mikos, A. G. *Biomaterials* **2007,** *28*, 4078. Published Online Jun 18, 2007.
16. Veetil, J. V.; Ye, K. *Biotechnol. Prog.* **2009,** *25*, 709.
17. Coleman, J. N.; Cadek, M.; Blake, R.; Nicolosi, V.; Ryan, K. P.; Belton, C.; Fonseca, A.; Nagy, J. B.; Gunk'ko, Y. K.; Blau, W. J. *Adv. Funct. Mater.* **2004,** *14*, 791.
18. Coleman, J. N.; Khan, U. M.; Gun'ko, Y. K. *Adv. Mater.* **2006,** *18*, 689.
19. Liu, T.; Phang, I. Y.; Shen, L.; Chow, S. Y.; Zhang, W. D. *Macromolecules* **2004,** *37*, 7214.
20. Mattioli-Belmonte, M.; Vozzi, G.; Whulanza, Y.; Seggiani, M.; Fantauzzi, V.; Orsini, G.; Ahluwalia, A. *Mater. Sci. Eng. C* **2012,** *32*, 152.
21. Popov, A. M.; Lozovik, Y. E.; Fiorito, S.; Yahia, L. *Int. J. Nanomed.* **2007,** *2*, 361.
22. MacDonald, R. A.; Laurenzi, B. F.; Viswanathan, G.; Ajayan, P. M.; Stegemann, J. P. J. *Biomed. Mater. Res. A* **2005,** *74*, 489.
23. Zanello, L. P.; Zhao, B.; Hu, H.; Haddon, R. C. *Nano. Lett.* **2006,** *6*, 562.
24. Supronowicz, P. R.; Ajayan, P. M.; Ullmann, K. R.; Arulanandam, B. P.; Metzger, D. W.; Bizios, R. J. *Biomed. Mater. Res.* **2002,** *5*, 499.
25. Whulanza, Y.; Ucciferri, N.; Domenici, C.; Vozzi, G.; Ahluwalia, A. *Biosens. Bioelectron.* **2011,** *26*, 3303.
26. Mariani, M.; Rosatini, F.; Vozzi, G.; Previti, A.; Ahluwalia, A. *Tissue Eng.* **2006,** *12*, 547.
27. Pantano, A.; Parks, D. M.; Boyce, M. C. J. *Mech. Phys. Solids* **2004,** *52*, 789.
28. Pioggia, G.; Di Francesco, F.; Marchetti, A.; Ferro, M.; Ahluwalia, A. *Biosens. Bioelectron.* **2007,** *22*, 2618.
29. Tirella, A.; Orsini, A.; Vozzi, G.; Ahluwalia, A. *Biofabrication* **2009,** *1*, 045002.
30. Vozzi, G.; Previti, A.; De Rossi, D.; Ahluwalia, A. *Tissue Eng.* **2002,** *8*, 1089.
31. Vozzi, G.; Previti, A.; Ciaravella, G.; Ahluwalia, A. J. *Biomed. Mater. Res. A* **2004,** *71*, 326.
32. Mattioli-Belmonte, M.; Vozzi, G.; Kyriakidou, K.; Pulieri, E.; Lucarini, G.; Vinci, B.; Pugnaloni, A.; Biagini, G.; Ahluwalia, A. J. *Biomed. Mater. Res. A* **2008,** *85*, 466.
33. Hicok, K. C.; Thomas, T.; Gori, F.; Rickard, D. J.; Spelsberg, T. C.; Riggs, B. L. J. *Bone Miner. Res.* **1998,** *13*, 205.
34. Thess, A.; Lee, R.; Nikolaev, P.; Dai, H.; Petit, P.; Robert, J.; Xu, C.; Lee, Y. H.; Kim, S. G.; Rinzler, A. G.; Colbert, D. T.; Scuseria, G. E.; Tomanek, D.; Fischer, J. E.; Smalley, R. E. *Science* **1996,** *273*, 483.
35. Mistry, A. S.; Mikos, A. G. *Adv. Biochem. Eng. Biotechnol.* **2005,** *94*, 1.
36. Xing, Q.; Zhao, F.; Chen, S.; McNamara, J.; Decoster, M. A.; Lvov, Y. M. *Acta Biomater.* **2010,** *6*, 2132.
37. Wang, Y.; Xia, H.; Zhao, Y.; Jiang, T. *IEEE Eng. Med. Biol. Soc. Conf.* **2005,** *5*, 4908.
38. Chrissafisa, K.; Antoniadisa, G.; Paraskevopoulosa, K. M.; Vassiliou, A.; Bikiarisb, D. N. *Compos. Sci. Technol.* **2007,** *67*, 2165.

39. Seitz, H.; Rieder, W.; Irsen, S.; Leukers, B.; Tille, C. J. *Biomed. Mater. Res. B* **2005,** *74*, 782.

40. Shalumon, K. T.; Chennazhi, K. P.; Tamura, H.; Kawahara, K.; Nair, S. V.; Jayakumar, R. *IET Nanobiotechnol.* **2012,** *6*, 16.

41. Wu, L.; Ding, J. *Biomaterials* **2004,** *25*, 5821.

42. Wu, L.; Ding, J. J. *Biomed. Mater. Res. A* **2005,** *75*, 767.

43. Lu, L.; Peter, S. J.; Lyman, M. D.; Lai, H. L.; Leite, S. M.; Tamada, J. A.; Vacanti, J. P.; Langer, R.; Mikos, A.G. *Biomaterials* **2000,** *21*, 1595.

44. Hutmacher, D. W. J. *Biomater. Sci. Polym. Ed.* **2001,** *12*, 107.

45. Montjovent, M.; Mathieu, L.; Hinz, B.; Applegate, L. L.; Bourban, P.; Zambelli, P.; Manson, J.A.; Pioletti, D. *Bone* **2005,** *36*, S278.

46. Montjovent, M. O.; Mark, S.; Mathieu, L.; Scaletta, C.; Scherberich, A.; Delabarde, C.; Zambelli, P. Y.; Bourban, P. E.; Applegate, L. A.; Pioletti, D. P. *Bone* **2008,** *42*, 554.

47. Zilberman, M.; Nelson, K. D.; Eberhart, R. C. J. *Biomed. Mater. Res. B* **2005,** *74*, 792.

48. Guarino, V.; Lewandowska, M.; Bil, M.; Polak, B.; Ambrosio, L. *Compos. Sci. Technol.* **2010,** *70*, 1826.

49. Even-Ram, S.; Artym, V.; Yamada, K. M. *Cell* **2006,** *126*, 645.

50. Kim, K. S.; Chae, Y. S.; Park, B. H.; Yoon, J. S.; Kang, M. S.; Jin, H. J. *Curr. Appl. Phys.* **2008,** *8*, 803.

51. Kuan, C. F.; Kuan, H. C.; Ma, C. C.; Chen, C. H. J. *Phys. Chem. Solids* **2008,** *69*, 1395.

52. Neumeister, J.; Jansson, S.; Leckie, F. *Acta Mater.* **1996,** *44*, 573.

53. Discher, D. E.; Janmey, P. A.; Wang, Y.-L. *Science* **2005,** *310*, 1139.

54. Roosa, S. M.; Kemppainen, J. M.; Moffitt, E. N.; Krebsbach, P. H.; Hollister, S. J. J. *Biomed. Mater. Res. A* **2010,** *92*, 359.

55. Murphy, C. M.; Haugh, M. G.; O'Brien, F. J. *Biomaterials* **2010,** *31*, 461.

56. Karageorgiou, V.; Kaplan, D. *Biomaterials* **2005,** *26*, 5474.